Lawrence Berkeley National Laboratory
Lawrence Berkeley National Laboratory

Title
An In-situ method for the study of strain broadening using synchrotronx-ray diffraction

Permalink
https://escholarship.org/uc/item/76g8h6fh

Authors
Tang, Chiu C.
Lynch, Peter A.
Cheary, Robert W.
et al.

Publication Date
2008-05-27

Peer reviewed

eScholarship.org Powered by the California Digital Library
University of California

An In-Situ Method for the Study of Strain Broadening using Synchrotron X-ray Diffraction

C.C. Tang[a], P.A. Lynch[b], R.W. Cheary[†c] and S.M. Clark[d *]

[a]Diamond Light Source, Chilton, Didcot, Oxfordshire OX11 0DE, UK, [b]CSIRO Manufacturing and Materials Technology, Gate 5, Normanby Road, Clayton, VIC 3168, Australia, [c]Department of Applied Physics, University of Technology, Sydney, Broadway, New South Wales 2007, Australia, [d]Advanced Light Source, Lawrence Berkeley National Laboratory, MS6R2100, 1 Cyclotron Road, Berkeley, CA 94720-8226, USA. Correspondence e-mail: smclark@lbl.gov

†Unfortunately R.W. Cheary passed away before this work was submitted for publication

A tensonometer for stretching metal foils has been constructed for the study of strain broadening in x-ray diffraction line profiles. This device, which is designed for use on the powder diffractometer in Station 2.3 at Daresbury Laboratory, allows in-situ measurements to be performed on samples under stress. It can be used for data collection in either transmission or reflection modes using either symmetric or asymmetric diffraction geometries. As a test case, measurements were carried out on a 18 μm thick copper foil experiencing strain levels of up to 5% using both symmetric reflection and symmetric transmission diffraction. All the diffraction profiles displayed peak broadening and asymmetry which increased with strain. The measured profiles were analysed by the fundamental parameters approach using the TOPAS peak fitting software. All the observed broadened profiles were modelled by convoluting a refineable diffraction profile, representing the dislocation and crystallite size broadening, with a fixed instrumental profile pre-determined using high quality LaB_6 reference powder. The de-convolution process yielded "pure" sample integral breadths and asymmetry results which displayed a strong dependence on applied strain and increased almost linearly with applied strain. Assuming

crystallite size broadening in combination with dislocation broadening arising from fcc a/2⟨110⟩{111} dislocations, we have extracted the variation of mechanical property with strain. The observation of both peak asymmetry and broadening has been interpreted as a manifestation of a cellular structure with cell walls and cell interiors possessing high and low dislocation densities.

Keywords: Line Broadening Analysis, Crystallite Size Determination, In-situ Strain Analysis, Synchrotron X-ray Diffraction.

---

* Corresponding author at: Advanced Light Source, Lawrence Berkeley National Laboratory, MS6R2100, 1 Cyclotron Road, Berkeley, CA 94720-8226, USA

Tel: 510 495 2442

E-mail address: smclark@lbl.gov

1. Introduction

Imperfections in materials can profoundly influence their mechanical, optical, magnetic and chemical properties. X-ray diffraction profiles from polycrystalline materials are broadened by atomic imperfections and deviations from ideal crystal structure. The analysis of line broadening is an important tool for studying imperfections and the microstructure associated with them as explained in the reviews by Langford (2000) and Ungár (2000). When a material is deformed or strained, the intensity distribution of the Bragg reflections can be affected in two ways. Firstly, the diffraction peaks may be shifted from their unstrained positions by the homogeneous strain while the peak shapes remain essentially unchanged. Secondly, both the breadth and the shapes of the peaks can change because of inhomogeneous strain. In cases where materials are under stress and particularly when experiencing plastic deformation, both kinds of strain occur together. Line broadening from strained materials is generally caused by either dislocation, stacking faults or lattice misfits between phases. In addition to strain broadening most materials also generate crystallite size broadening which arises from the finite thickness of the crystals in the direction $\boldsymbol{d}^*_{hkl}$ of domains over which diffraction is coherent. This is readily detectable once the crystallite size is in the sub-micron range. References related to these topics are cited in the reviews mentioned above. As these effects are usually concomitant, methods have been developed to measure the individual sources of broadening (Warren-Averbach, 1950; Williamson & Hall, 1953; Warren, 1959). In the present work the broadening arises primarily from dislocations, but some crystallite size broadening is also detected.

According to Krivoglaz (1996), dislocations or dislocation-type lattice defects are second class (or class II) defects with a long range strain gradient that produces x-ray line broadening. Since dislocations are anisotropic linear lattice defects, the magnitude of the broadening or "contrast" depends on the type of dislocation and on the direction of the diffraction vector relative to the Burgers vector of the dislocation. The term contrast factor or orientation factor, which reflects the

hkl dependence of dislocation broadening, was introduced by Wilkens (1970) and Krivoglaz *et al.* (1983), and further developed by Wilkens (1987), Kužel & Klimanek (1988, 1989) and Klimanek & Kužel (1988). More recently, Ungár & Borbély (1996), Ungár *et al.* (1998) and Wu *et al*. (1998) have introduced analytical methods to determine dislocation parameters with the orientation taken into account. The anistropy of the broadening with *hkl* is an indicator of the type of dislocation (i.e. edge, screw or mixed) whilst the shape of the diffraction profiles is an indicator of the interaction and distribution of the dislocations. It is possible to determine the dislocation density from the integral breadth β^* (in reciprocal lattice units), provided the type of dislocation in the material is known, using the relationship,

$$\beta^* = \frac{bd^*_{hkl}}{2}\sqrt{C_{hkl}\rho\, f(M)} \tag{1}$$

where b is the magnitude of the dislocation Burgers vector, ρ is the total dislocation density, f(M) is a statistical parameter characterising the interaction and distribution of dislocations in an ensemble (Wilkens, 1970, 1976; Wu *et al*. 1998), and C_{hkl} is the 'contrast factor' or 'orientation factor'. Together, d^*_{hkl} and C_{hkl} determine the anisotropy of β^* with *hkl*. In turn the magnitude of C_{hkl} and its variation with *hkl* is dependent on the type of dislocation and the active slip system. For this reason the contrast factors are of central importance in the interpretation of dislocation broadening. In any analysis of dislocation broadening the contrast factors C_{hkl} have to be calculated for a particular model. The model is then evaluated by plotting β^* against $d^*_{hkl}\sqrt{C_{hkl}}$ (see for example, Ungár *et al.*, 1998; Ungár & Tichy, 1999) which, if valid, will be a straight line passing through the origin assuming there is no crystallite size or stacking fault broadening in the diffraction profiles. If however the presence of crystallite size and dislocation are additive (i.e. Lorentzian profile shape), then Eq. 1 is modified and expressed as:

$$\beta^* \approx \frac{1}{\tau_{app}} + d^*_{hkl}\sqrt{\frac{b^2 f(M) C_{hkl}\rho}{4}} \qquad (2)$$

where τ_{app} is the apparent crystallite size. When only the same set of planes over several orders of reflection (e.g. 200, 400 and 600) is considered, a plot of β^* against d^*_{hkl} at each strain can be used to determine the apparent crystal size τ_{app} and the total dislocation density ρ provided the orientation factor, C_{hkl} and interaction term $f(M)$ are known. As for the contrast factor C_{hkl} Eqs.1 and 2 is the same for each line in a multiple order set and tabulated values are available for Cu (Wilkens, 1987; Ungár *et al.*, 1998), the determination of τ_{app} and the dislocation density $\rho_f = \rho b^2 f(M)/4$ is more straightforward, with $C_{h00} \approx 0.305$ for three difference dislocation types: (i) 100% screw, (ii) 100% edges and (iii) the edge and screw dislocations are present with equal probability.

X-ray line profile studies of the dislocation structure in tensile-deformed Cu single crystals oriented for single slip have been reported by Wilkens *et al*. (1980) and Ungár *et al.* (1982). Following this, analytical procedures were developed by Groma *et al.* (1988) and Ungár *et al*. (1989) for interpreting the asymmetric broadening which arises from the heterogeneous distribution of the dislocations within plastically deformed solids. In the present study, it was shown that the results could be explained in terms of a dislocation cell structure first developed by Mughrabi (1983) where the cell walls have very high dislocation densities up to ten times the dislocation density of the cell interiors.

2. Analytical Procedure and Present Aim

In order to yield useful mechanical information, analytical procedure to refine our data has been developed to yield quantitative results. The development is described in detail in our previous publication (Cheary *et al.*, 2001). Here we describe the main features in the analysis.

The observed profile for a given reflection, B(2θ) is a convoluted function expressed as

$$B(2\theta)=S(2\theta)\otimes I(2\theta) \quad (3)$$

where S(2θ) and I(2θ) are the contributions from the sample and the instrument respectively. Clearly, to extract structural information in B(2θ) the procedures of de-convolution must be undertaken. Before the measurements of Cu specimens, line profiles were collected from a high quality LaB_6 powder with a negligible microstructure effect, a reference material from the National Institute of Standards and Technology (NIST). More than 20 reflections from the primitive cubic material (a=4.569 Å) were obtained from 20º to 120º (2θ). The modelling of the instrumental contribution was performed using the TOPAS software (Bruker AXS). This program uses a fundamental parameters approach to the fitting (Cheary & Coelho, 1992; Cheary & Coelho, 1998) which allows profiles to be expressed in terms of instrument related parameters and enables instrument profiles to be generated at any 2θ angle from the fitted parameters. Subsequent profile fittings were performed using this software. All the observed broadened profiles B(2θ) were modelled by convoluting a refineable diffraction profile S(2θ), representing the dislocation and crystallite size contribution, with a fixed pre-determined I(2θ) calculated using the refined instrument parameters from the reference LaB_6 profiles (see Cheary *et al.*, 2001). The diffraction profile S(2θ) was modelled as a convolution of a Lorentzian L(2θ) and a Gaussian G(2θ) function to represent the symmetrical broadening, and an exponential function E(2θ) to account for the observed asymmetry. The refineable parameters in S(2θ) were the full widths at half maximum intensity (Lorentzian and Gaussian component) and the asymmetry parameter, δ. The integral breath $\beta_{2\theta}$ determined from the fitted profile S(2θ) was converted to β^* (= $\beta_{2\theta}\cos\theta/\lambda$) in reciprocal lattice units ($Å^{-1}$) which was used as a measure of the observed line broadening. The asymmetry

arising from the strained profile is represented by the asymmetry shift ΔS, quantified by the difference between the angles of peak maximum and the centroid of S(2θ).

Most recent studies on dislocation broadening from polycrystalline materials have focused on materials with some form of inhomogeneous residual strain but without any applied stress. The principle objective of the present investigation is to extend the scope of strain broadening analysis by studying metal foils under an applied stress during measurement using a high resolution synchrotron based diffractometer. By carrying out in-situ studies of this type, new relationships may be revealed between the mechanical behaviour and the line profile characteristics over the whole of the deformation spectrum from the elastic to plastically deformed regions. The addition of an applied uni-axial tensile stress produces both tensile and compressive stresses in metal foils, parallel and perpendicular to the tensile axis respectively. With a parallel beam synchrotron system it is possible to study how the line broadening and line shape change as the direction of the diffraction vector is varied with respect to the direction of applied stress. Unlike the conventional divergent beam diffractometer, it is possible to use either transmission or reflection diffraction geometries without loss of resolution and to tune the wavelength to minimise absorption losses. More importantly, in oriented metal foils it is also possible to collect all the *hkl* lines from crystallites with the same orientation within the foil by using asymmetric diffraction conditions rather from crystallites with different orientations as in the normal θ-2θ mode of data collection.

3. Instrumental

3.1 Sample stretching mechanism - Tensonometer

The key developed component of the work is the tensioning device built for use on a synchrotron powder diffraction beamline. The tensonometer was designed and constructed purposely to stretch metal foils. To provide mechanical strength and rigidity, the body of the device consists of a metal

frame made of 12 mm thick steel. The height, width and length of the frame are approximately 6, 11 and 40 cm respectively. With one of the two clamps placed on the stretching axis is adjustable by a worm gear shaft. The stretching of the sample was achieved by changing the separation of the clamps with a high ratio gearbox driven by a stepper motor. A resolution of 3000 steps per mm allows for precise control of the sample stretching. The sample extension can be accurately monitored with a high precision gauge (Sylvac80) which has a resolution of ±0.1 μm. An accuracy of ±1μm was achieved by monitoring a sample under tension for 12 hours. The highly parallel x-ray beam produced by a synchrotron source could only sample a small number of crystallites in diffraction position at one time. This under sampling can give poorly defined peak profiles. In order to overcome this problem, the stretching frame is mounted on an oscillatory translator (~2 Hz) with a displacement of 3 cm parallel to length of the foil. The oscillation ensured that the beam samples sufficient crystallites in the diffraction condition to produce smooth profiles.

During the experiment, the entire stretching device, which weighs approximately 10 kg, was mounted on the θ-circle of the diffractometer as shown in Fig. 1 for both reflection and transmission modes. The top surface of the metal foil was optically aligned to be at the centre of rotation of the diffractometer and was adjustable with an offset screw mechanism. The transmission mode can be readily achieved by a rotation -90º of the θ-circle (redefined as zero) as shown in Fig. 1 (bottom). When the stretching device is operating in reflection mode, diffraction data collected by symmetrical scanning (θ-2θ) are from crystal planes parallel with the sample surface. In the same fashion, structure details from lattice planes normal to the surface can be obtained with use of the transmission geometry. The loaded foil shown is gripped by the two clamps which can be driven apart remotely to provide tensile stress.

3.2 Powder diffraction beamline – Station 2.3 at SRS

Station 2.3 is situated approximately 15 m tangentially from a 1.2 T bending magnet in the storage ring which confines a 2 GeV electron beam. The beamline receives x-rays from the synchrotron in the range of λ= 0.5-3.0 Å and the maximum x-ray flux at the station is approximately 10^9 photons/mm^2/s at wavelengths between 1.2 Å and 1.5 Å. The diffractometer on this station, which is shown in Fig. 1, was built initially for ambient conditions high-resolution powder diffraction (Cernik *et al.* 1990 and Collins *et al.* 1992). The "white" beam from the synchrotron is monochromatised by a channel-cut Si(111) single crystal maintained at 30.0±0.1ºC to achieve thermal stability. Two pairs of centre opening slits define the monochromatic beam incident at the centre of the two circle (θ-2θ) diffractometer and adjustable slit jaws allow the size of the incident beam to be set before the experiment. A scintillation detector mounted below the beamline, is used to monitor the incident x-ray flux using a kapton foil set obliquely between the monochromator and the centre of the diffractometer (sample position).

With the high flux, wavelength tuneability and parallel beam optics, the station is routinely used for structural studies of polycrystalline materials in several diffraction geometries (Tang *et al.*, 1998). The instrument has the flexibility for fast hardware re-configuration and adaptation, so that a variety of experiments can be performed. The incorporation of the tensonometer for the present in-situ experiment is further example of the instrument's flexibility. The commonly used geometry on this station is the flat-plate sample, long parallel foils configuration first developed by Hart & Parrish (1986) and Parrish *et al*. (1986). In this arrangement the diffracted beam from the sample at the centre of the θ-circle is collimated by equatorial Soller slits with an overall aperture of 25x25 mm^2 and an acceptance angle $\Delta 2\theta \approx 0.06°$. A set of short longitudinal foils is added to the collimation for the reduction of axial beam divergence. The collimating characteristics of the parallel foils are given in detail by Roberts & Tang (1998). To minimise absorption and scattering of the beam, the long equatorial Soller slit assembly is permanently evacuated during data

collection. A low noise enhanced dynamic range detector at the other end of the foils records the diffraction count rate.

4. Experimental

Specimens were prepared from 18 μm thick Cu foil with a purity of 99.99%. The foil possess a strong (100) texture perpendicular to the surface with sub-micron grain size. Also the [001] is parallel to the rolling direction. Each diffraction specimen was cut from a large sheet as a strip 200 mm long (in the rolling direction) and 22 mm wide. The strips were then rolled lightly to remove irregularities and annealed at 400ºC in vacuum ($<10^{-6}$ mbar) for 4 hours. Each specimen was then loaded onto the tensonometer and held by the clamps which were set at an initial separation of 100 mm.

An incident beam of 2 mm (vertical) by 10 (horizontal) mm was used to give a large illuminated area on the specimen. The wavelength and 2θ calibrations were performed using the first 9 reflections from high quality silicon powder (640b) supplied by NIST. The calibrated wavelength used in our experiment was λ=0.70022(5) Å, where the value in brackets represents the uncertainty in the last decimal place. A short wavelength was used to minimise absorption for data collected in transmission mode. Peak profiles were measured using symmetrical scanning (θ/2θ) with the diffraction vector either perpendicular to tension axis (reflection mode) or parallel to the tension axis (transmission mode). Two sets of profile data were collected for each of these modes. First, the multiple order Bragg reflection 200, 400 and 600 were scanned alternately in the transmission and reflection modes starting at zero strain and then at increasing strain levels up to 5 mm. At low strains this was done in discrete steps of 100 μm increasing to 0.5-1.0 mm at higher strain levels. In all cases the profiles were step scanned individually over an adequate range in 2θ using step sizes of either 0.005º for sharper lines or 0.01º 2θ for broader lines. The

measurement time was chosen to give at least $10x10^3$ and $3x10^3$ counts at the peak maximum for the strong and weak peaks respectively. A few reflections were measured with λ=1.00535(5) Å.

High background levels arising from Cu K fluorescence increased the background to peak ratio at the 600 reflection to ~0.4. Although some improvement was obtained by optimising the pulse height analysis electronics, considerable reduction of the background was realised by putting a thin 15µm Co foil in the diffracted beam. This measure improved the peak to background ratio by a factor of 10. A longer wavelength above the K absorption edge of copper could have been selected to avoid fluorescence, but this was an undesirable option since a longer wavelength would be heavily attenuated in the transmission mode, and prevented accessibility to higher order peaks.

5. Results and discussions

5.1 Profile assessment

With the use of the oscillator to sample more crystallites, the improvement to the peak profile definition is clearly shown in Fig. 2. The 600 reflection were taken without oscillation (open circles) illustrating doubled peaks, while the data (filled circles) with oscillation can be adequately fitted with a standard analytical function (pseudo-Voigt was used in this case) shown as single profile. Both data sets were collected using θ-2θ scan with a step size of 0.01° and 5 second per step (λ=1.00535 Å). Fig. 3 shows examples of the profile broadening generated by the tensioning of the Cu foil. With zero stress, only crystallite size (typical size ~ 0.2-0.5 µm) contributed to the slight broadening. On the application of stress to the specimen, all the profiles undergo shifts and are also broadened once a sufficient amount of stain has been applied. However, the peak shift and broadening occurred more rapidly with applied strain in the transmission case. Both transmission (tension) and reflection (compressive) profiles become increasingly asymmetric with strain increase, but in the opposite direction (Fig. 3). These changes reflect the facts: (i) in the

transmission case the observed change in profile shape is due to tensile strain, (ii) in the reflection case the broadenings are due to the compressive structural changes perpendicular to the tensile direction.

Following the analytical procedure described in Section 2, excellent fits were obtained to all observed profiles with the weighted R-factor typically in the range 2-3%. Fig. 4 show examples of results obtained from the analysis. The reflection and transmission measurements were done with the Cu specimen under 3% and 4.5% strain respectively. The increase in the breadth and asymmetry with applied strain are clear as presented in Fig. 5; the 600 profiles are shown since it has the most noticeable effect. The line profile shape changes significantly once the strain exceeds 0.2% (elastic limit).

The results of β* for 200, 400 and 600 peak are plotted as a function of K ($d^*\surd C_{h00}$) for both the compression and tension data (Fig. 6). For qualitative analysis, three sets of data are illustrated in each case to show the variation of the slope and intercept with applied strain. Using Eq.2, we can extract mechanical information from these plots. First, the points of interception are at $\beta_0^* \sim 0.3$ to $0.5\text{x}10^{-2}$ nm^{-1} giving an apparent crystallite size τ_{app}~0.25 μm from both measurements. Secondly, the slope (proportional to dislocation density ρ_f) increases with specimen extension for both cases but more so in tension. Due to the profile asymmetry (Fig. 5b), however, additional considerations in our analytical procedures were taken as described below to properly extract the dislocation densities.

5.2 Additional Analysis

Asymmetry broadening of the diffraction profiles is an indication of the inhomogeneity of the dislocations within copper crystallites arising from dislocation pile-up. Some regions are heavily

deformed with high dislocation density whereas other regions are less deformed possessing a lower dislocation density. Although a general model for interpreting this behaviour has been developed (Groma *et al*., 1988) it is somewhat difficult to implement and as such we have implemented the quasi-composite model first used by Ungár *et al.* (1984). In this model a measured profile is decomposed into two components representing contributions from the high and low density regions. The shape and breadth of these component profiles is then analysed separately using the line broadening model of Wilkins (1970, 1976). In previous studies and recent work by Breuer *et al.* (2000), these two regions were described by a cellular structure (Mughrabi, 1983) with cell walls and cell interiors possessing high and low dislocation density, respectively as shown in Fig. 7a.

Before this work the quasi-composite model had only been applied to single crystal data from a very high resolution, special purpose instrument. In our work, we are applying the method to a polycrystalline sample using a medium resolution instrument by comparison. Under these circumstances, the refinement procedure is susceptible to systematic errors because the profile parameters for defining the component fitted profiles within a measured profile are not unique under unconstrained refinement. For an accurate refinement, a heavily constrained refinement procedure was developed. This was based on refining six profiles simultaneously namely 200, 400 and 600 profiles in both transmission and reflection modes at each strain level. Fig. 7 shows the double peak model used to fit the observed profiles. The constrains implemented in the present fitting procedure at each applied strain included: (a) The volume fraction of the cell walls, given by the ratio of the integrated intensities of the components, is the same for all six profiles, (b) The spacing between each doublet represents a constant difference in d space. The difference is not the same for compression and tension profiles. (c) The profile shape, representative of the Voigt shape factor, is the same for all cell wall profiles. Similarly, all the profiles from the cell interiors have the same shape. The outcome of this analysis is illustrated in Fig. 8 in terms of the lattice parameters (a) in the cell interiors and walls of copper under strain and the dislocation densities

(ρ_f) at each of these regions. There are clear differences in the calculated lattice parameters between the cell interiors and cell walls, in particular when the crystallites were under tension. This is in agreement with the cellular model. That is, the regions of high strain (cell walls) in both compression and tension represent the maximum observed lattice parameter shift, whereas the cell interiors (regions of lower defect density) the magnitude of the lattice parameter shift is reduced.

The average dislocation densities determined in this work are of the order of 10^{13} m^{-2}. This is lower than the values determined in previous studies (Ungár et al. (1984, 1989) and Breuer et al. (2000)). This is probably due to the fact that our samples were well annealed foils while the other studies used plastically deformed single crystals or nano-particles. This suggests that the defect densities that we measure might represent the lower bound of the range of possible defect densities that might be observed in a copper sample. While the dislocation density for the cell interiors is seen to vary almost linearly with applied strain. The densities determined for the cell wall have a much higher degree of scatter due to the fact that the contribution to the diffraction profile from the walls is much weaker than from the interior.

6. CONCLUSIONS

The tensonometer constructed for the in-situ measurements has been successfully commissioned in Station 2.3. Good quality diffraction peaks of strain copper foils (0-5%) were collected from crystal planes parallel (reflection mode) and orthogonal (transmission mode) with the direction of applied stress. With the instrumental contribution accounted for using fundamental parameters approach facilitated in the TOPAS software, the integral breadths and lattice parameters of the de-convoluted profiles (pure sample contribution) were extracted. The broadening of the breadths and the development of peak asymmetry were clearly observed, even in profiles at strain below the elastic limit of the material. The breadth and asymmetry parameters were then characterised as a function of applied strain. With the application of stress, the development of dislocations in the Cu

sample is clearly evident. Analyses have yielded an apparent crystallite size of ~0.25 μm which changes little with applied strain. However, both the reflection and transmission results show that the lattice parameter and dislocation density (ρ) vary considerably with applied load. Further development of data analysis assuming the quasi-composite dislocation model of a cellular crystallite has yielded results for lattice parameters and dislocation density as a function of applied load. There are clear differences in the structural properties between the cell interiors and cell walls even when the specimen was under low strain (0.3-1%). At high strain (3-5%), a difference of Δa=0.003 Å has been recorded for the lattice parameters under tension between the two regions and an increase of dislocation density (ρ_A) by a factor of two in the cell wall has been observed.

The present study has clearly demonstrated that the changes in micro-structures can be obtained from the copper foils using the newly commissioned device on the synchrotron powder diffraction beamline. The device was also designed to allow asymmetrical profiling, well suited to the study of defects in anisotropic crystal structures. The examination of the orientation dependence and detailed profiling during strain relaxation are two possible studies which have immediately been raised from this investigation. The in-situ technique has also opened the possibility to investigate dislocation systems in other metals.

Acknowledgements

We would like to acknowledge the technical team at Daresbury Laboratory for their assistance in the construction of the tension device and their support during the beamtime. Our thanks also go to EPSRC (UK) for the provision of the project fund (Grant No. GR/M31163). The Advanced Light Source is supported by the Director, Office of Science, Office of Basic Energy Sciences, of the U.S. Department of Energy under Contract No. DE-AC02-05CH11231.

References

Breuer, D., Klimanek, P., & Pantleon, W. (2000), J. Appl. Cryst. **33** 1284-1294.

Cernik, R.J., Murray, P.K., Pattison, P. & Fitch, A.N. (1990). J. Appl. Cryst. **23**, 292-296.

Collins, S.P., Cernik, R.J., Pattison, P., Bell, A.T.M. & Fitch, A.N. (1992). Rev. Sci. Instrum. **63**, 1013-1014.

Cheary, R.W & Coelho, A.A. (1992), J. Appl. Cryst. **25**, 109-121.

Cheary, R.W & Coelho, A.A. (1998), J. Appl. Cryst. **31**, 862-868.

Cheary, R.W., Tang, C.C., Lynch, P., Roberts, M.A. & Clark, S.M. (2001). Mater. Sci. Forum **378-381**, 358-363.

Groma, I., Ungár, T. & Wilkens, M. (1988). J. Appl. Cryst. **21**, 47-53.

Hart, M. & Parrish, W. (1986). Mater. Sci. Forum **9**, 39-46.

Krivoglaz, M.A (1996). *X-ray and Neutron Diffraction in Nonideal Crystals*, Springer-Verlag, Berlin, p. 357-420.

Krivoglaz, M.A., Martynenko, O.V. & Ryaboshapka, K.P. (1983). Fiz. Metall. Metallov. **55**, 5-17.

Klimanek, P. & Kužel, R. Jr (1988). J. Appl. Cryst. **21**, 59-66.

Kužel, R. Jr & Klimanek, P. (1988). J. Appl. Cryst. **21**, 363-368.

Kužel, R. Jr & Klimanek, P. (1989). J. Appl. Cryst. **22**, 299-307.

Langford, J.I. (2000). *Industrial Applications of X-ray Diffraction*, edited by F.H. Chung & K. D.K. Smith, p751-775, Marcel Dekker, New York.

Mughrabi, H. (1983). Acta Metall. **31**, 1367-1379.

Parrish, W., Hart, M., Erickson, C. G., Masciocchi, N. & Huang, T. C. (1986). Adv. X-ray Anal. **29**, 243-250.

Roberts, M.A. & Tang, C.C. (1998). Synchrotron Rad. **5**, 1270-1274.

Tang, C.C., Miller, M.C. & MacLean, E.J. (1998). Technical Report, DL-TR-98-001, CLRC Daresbury Laboratory, UK.

Ungár, T. (2000). *Industrial Applications of X-ray Diffraction*, edited by F.H. Chung & D.K. Smith, p847-867, Marcel Dekker, New York.

Ungár, T. & Borbély, A. (1996). Appl. Phys. Lett. **69**, 3173-3175.

Ungár, T, Groma, I. & Wilkens, M. (1989). J. Appl. Cryst. **22**, 26-34.

Ungár, T., Mughrabi, H., Rönnpagel, D & Wilkens, M. (1984). Acta Metall. **32**, 333-324.

Ungár, T., Ott, S., Sanders, P.G., Borbély, A. & Weertman, J.R. (1998). Acta Mater. **46**, 3693-3699.

Ungár, T., Révész, Á. & Borbély, A. (1998). J. Appl. Cryst. **31**, 554-558.

Ungár, T. & Tichy, G. (1999). Phys. Stat. Sol. **171**, 425-434.

Warren, B.E. (1959). Progr. Metal Phys. **8**, 147-202.

Warren, B.E. & Averbach, B.L. (1950). J. Appl. Phys. **21**, 595-599.

Wilkens, M. (1970). Phys. Stat. Sol. (a) **2**, 359-370.

Wilkens, M. (1976). Krist. Tech. **11**, 1159-1169.

Wilkens, M. (1987). Phys. Stat. Sol. (a) **104**, K1-K6.

Wilkens, M., Herz, K. & Mughrabi, H. (1980). Z. Metallkd. **71**, 376-384.

Williamson, G.K. & Hall, W.H. (1953). Acta Metall. **1**, 22-31.

Wu, E., Mac A. Gray, E. & Kisi, E.H. (1998). J. Appl. Cryst. **31**, 356-362.

Figure Captions

Figure 1. The tensonometer at reflection (top) and transmission (bottom) mode on Station 2.3 diffraction instrument. Cu foil specimen loaded at the centre of instrument.

Figure 2. The copper 600 peak measured without (a) and with (b) sample oscillation. The profiles were measured (circles) at reflection geometry with an x-ray beam of λ=1.00535 Å. The solid line in (b) is the fitted results to the observed data using pseudo-Voigt function. The intensity scale of (b) has been shifted up for clarity.

Figure 3. The 600 reflection measured at 0% (dashed curve) and 5% applied strain (solid circles – reflection and solid squares - transmission) at λ=0.70022(5) showing the effect of stress on the profile shapes.

Figure 4. The 600 observed profile (open circle), fitted data (solid curve) and the difference (grey curve) measured using transmission geometry with λ=0.70022 Å (main plot) and reflection geometry with λ=1.00535 Å (inset).

Figure 5. The increase in FWHM (a) and the asymmetry shift (b) of the 600 line as a function of applied strain relative to the 600 line at zero strain.

Figure 6. Variation of integral breadth (β^*) with K ($d^*\sqrt{C_{h00}}$) measured in 200, 400 and 600 profile (a) reflection and (b) transmission.

Figure 7. (a) Depicted single crystallite showing idealised representation of the cellular structure arising when dislocation pile-up occurs in cell walls. (b) Double peak model to fit cellular

dislocation arrangement depicted in (a) with one profile representing the cell walls and the other cell interiors.

Figure 8. (a) Lattice parameter of the copper foil under stress in regions of low (cell interiors) and high (cell walls) dislocation densities: (i) cell walls in tension, (ii) cell interiors in tension, (iii) cell interiors in compression, (iv) cell walls in compression. (b) Average dislocation density in the cell interiors and cell walls as a function of applied strain. The corresponding solid line is the linear fit of the data.

Figures in Tang *et al* (2006)

Figure 1

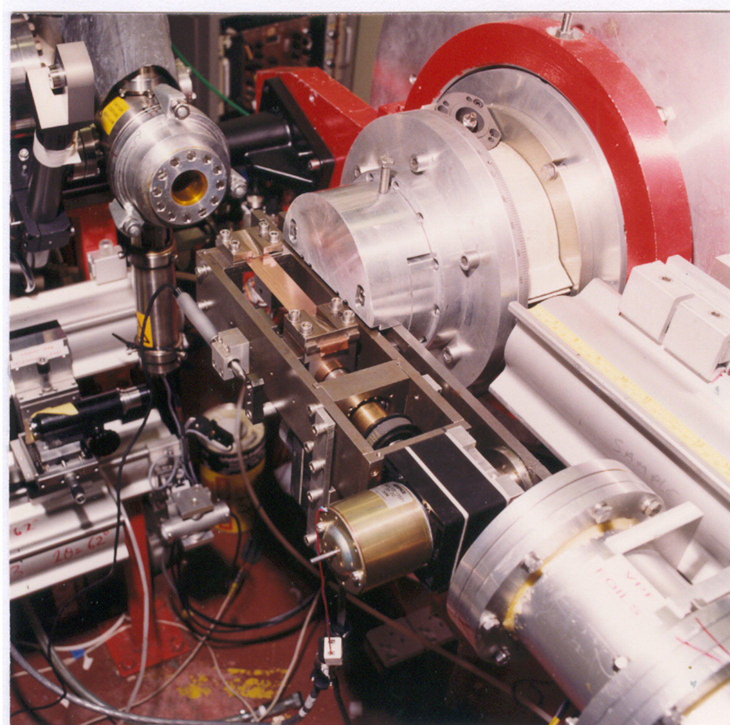

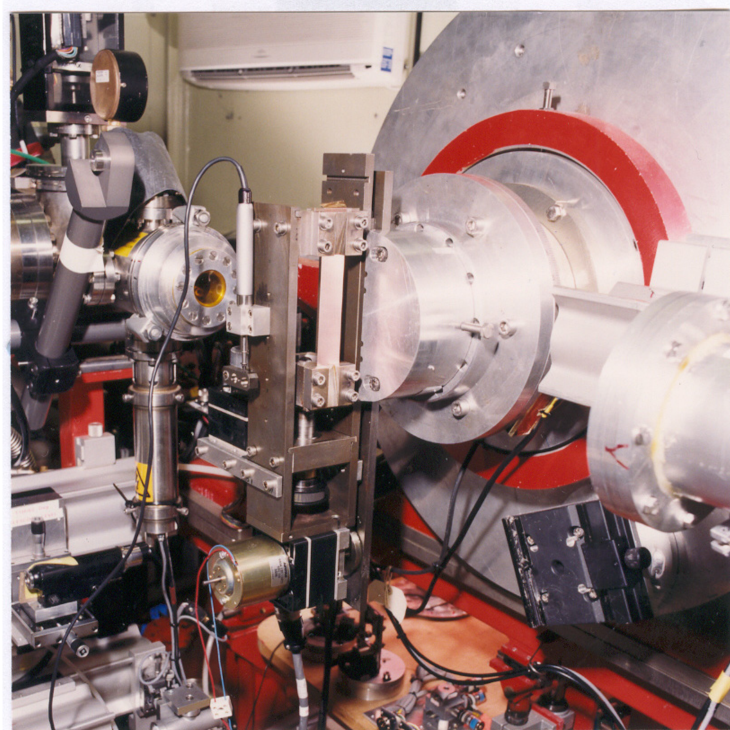

Figure 2

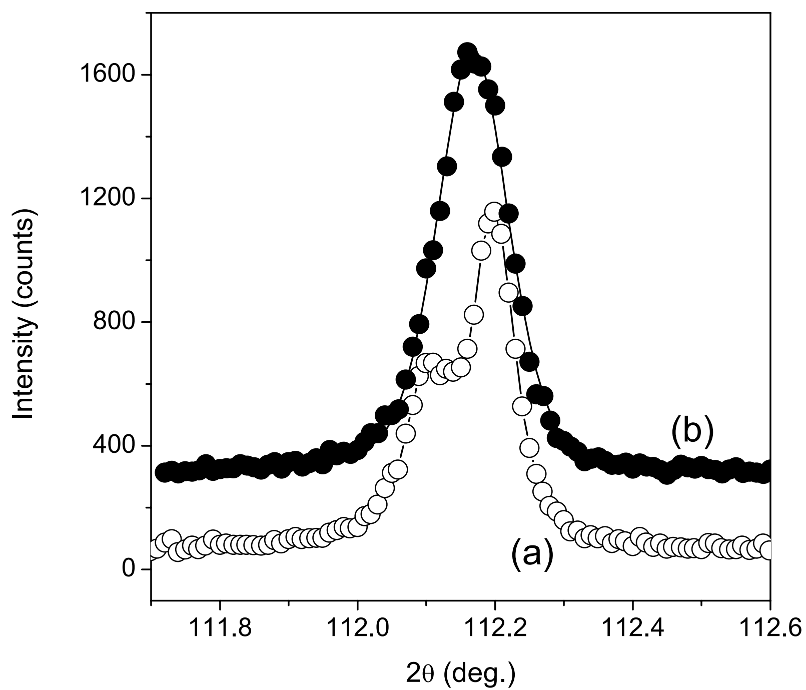

Figure 3

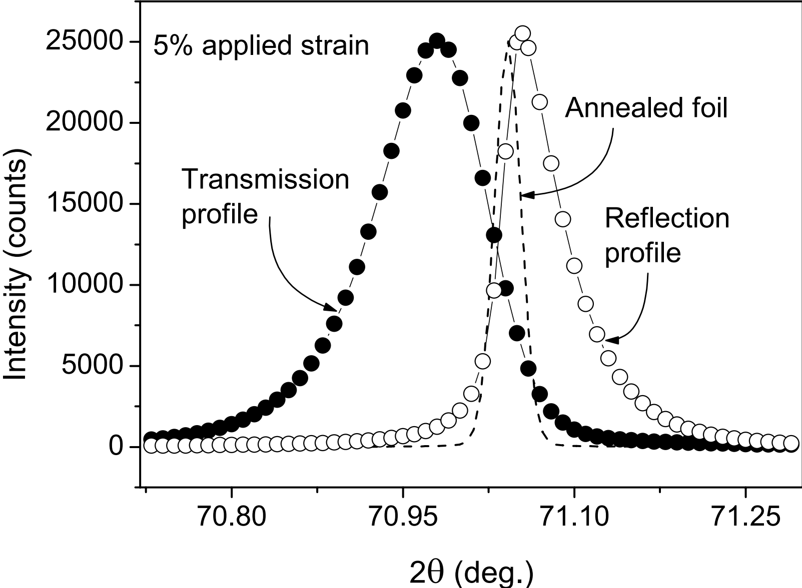

Figure 4

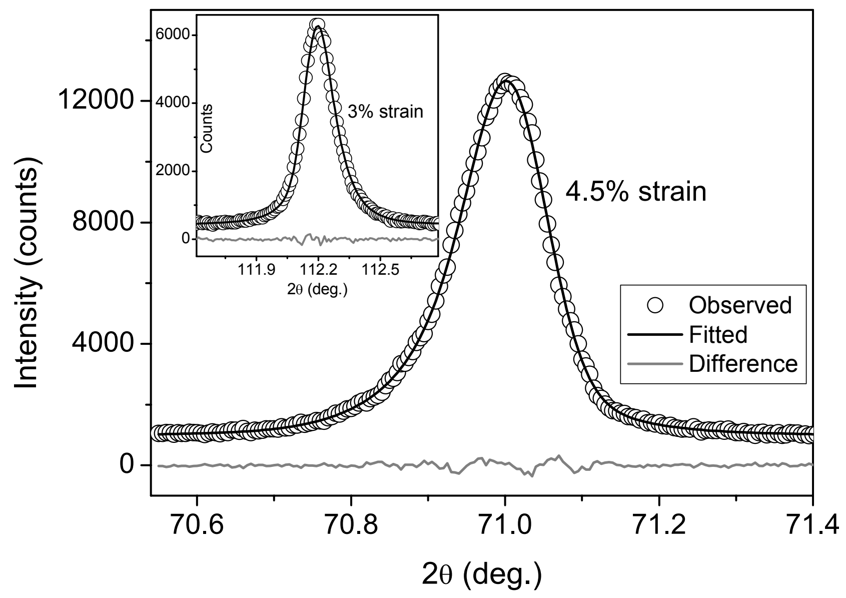

Figure 5

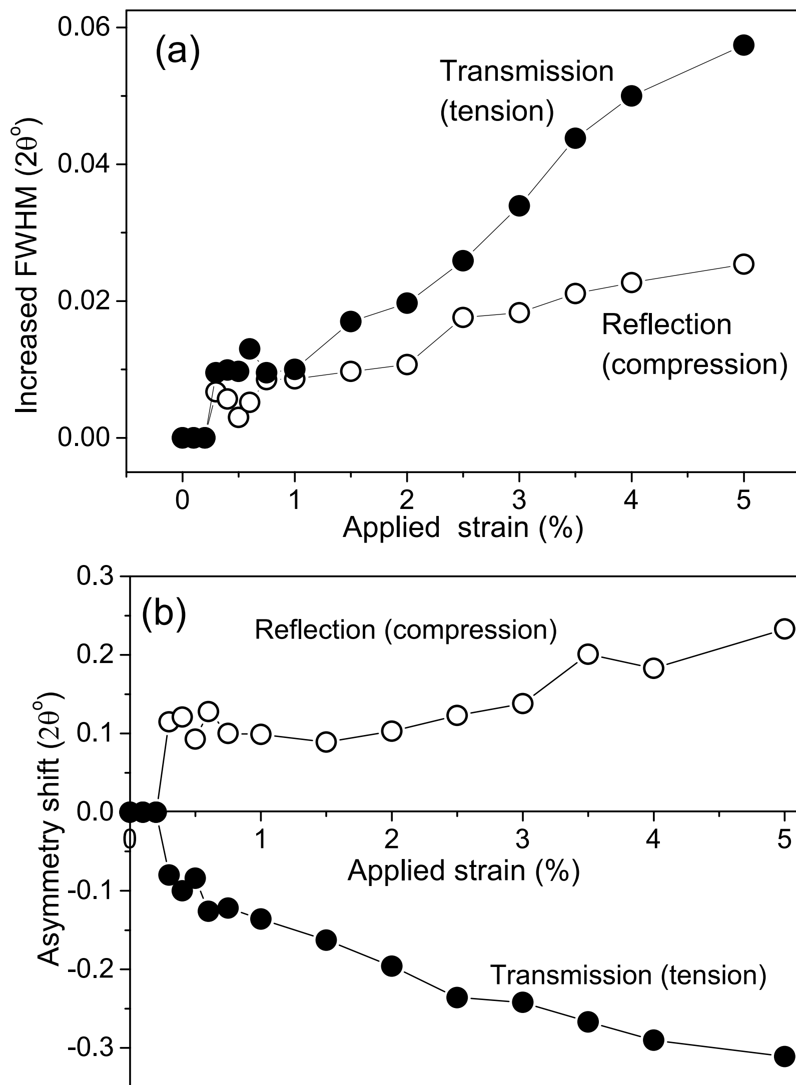

Figure 6

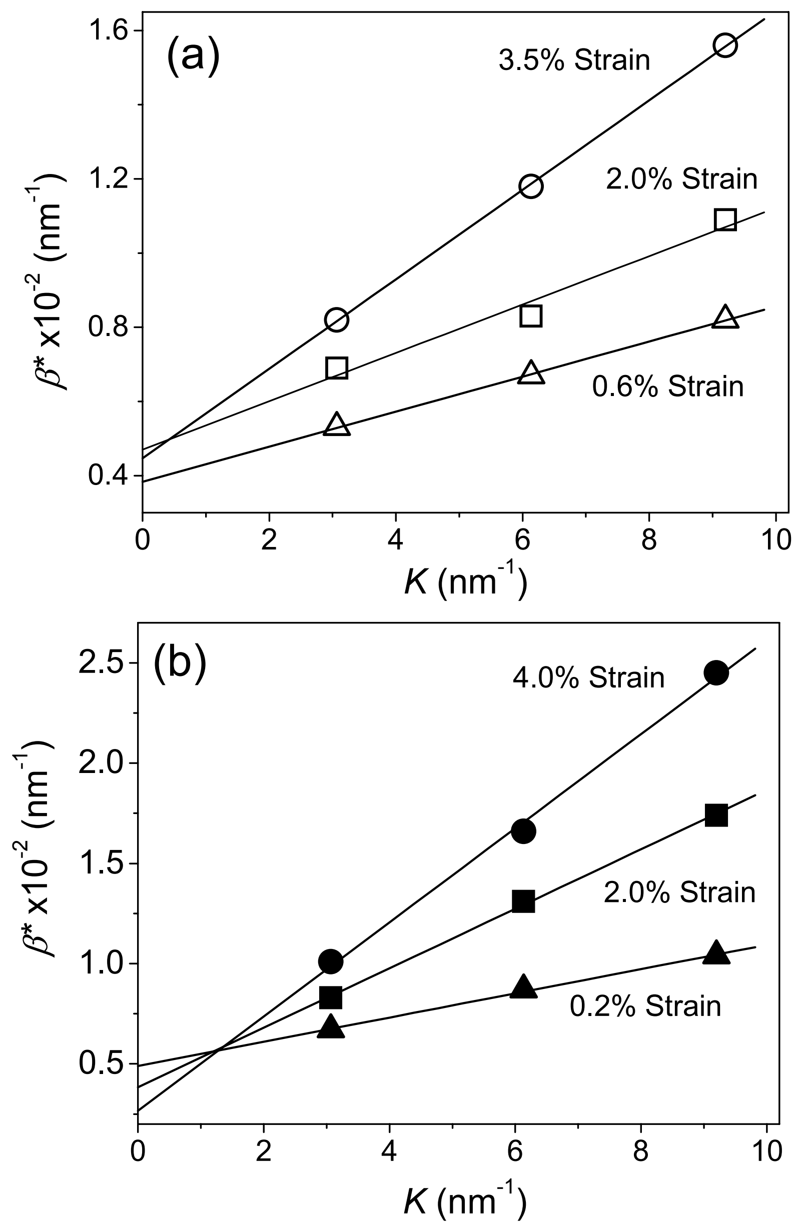

Figure 7

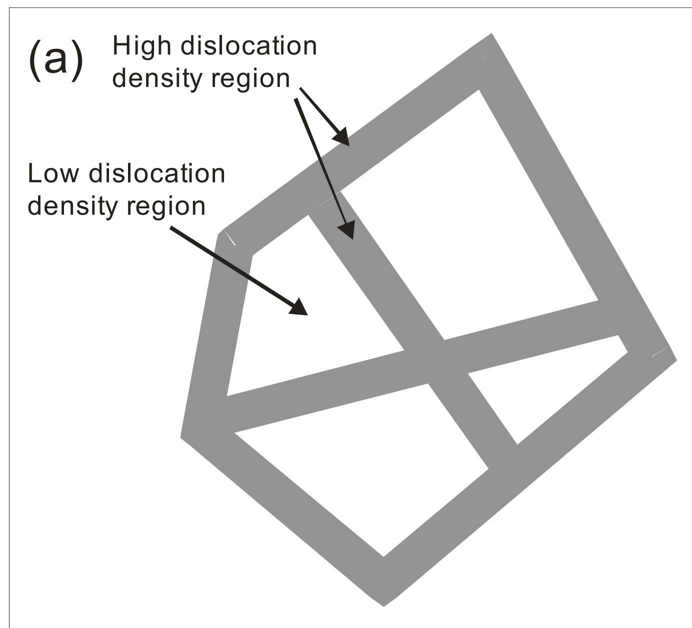

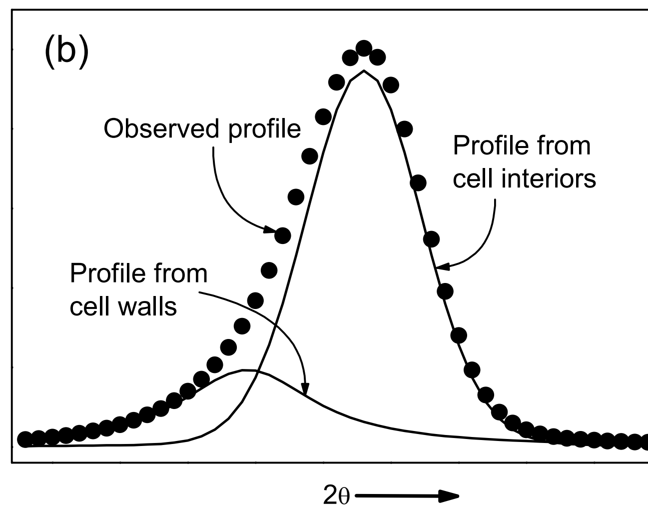

Figure 8